Mon. Not. R. Astron. Soc. **349,** 882–888 (2004) doi:10.1111/j.1365-2966.2004.07559.x

Modelling the two-point correlation function of galaxy clusters in the Sloan Digital Sky Survey

Spyros Basilakos[1]★ and Manolis Plionis[1,2]

[1]*Institute of Astronomy & Astrophysics, National Observatory of Athens, I. Metaxa & V. Pavlou, Palaia Penteli, 15236 Athens, Greece*
[2]*Instituto Nacional de Astrofisica, Optica y Electronica (INAOE), Apartado Postal 51 y 216, 72000, Puebla, Pue., Mexico*

Accepted 2003 December 16. Received 2003 December 16; in original form 2003 April 30

ABSTRACT

We study the clustering properties of the recently compiled Sloan Digital Sky Survey (SDSS) cluster catalogue using the two-point correlation function in redshift space. We divide the total SDSS sample into two richness subsamples, roughly corresponding to Abell $R \geqslant 0$ and Automated Plate Measuring (APM) clusters, respectively. If the two-point correlations are modelled as a power law, $\xi(r) = (r_0/r)^\gamma$, then the best-fitting parameters for the two subsamples are $r_0 = 20.7^{+4.0}_{-3.8}\ h^{-1}$ Mpc with $\gamma = 1.6^{+0.4}_{-0.4}$ and $r_0 = 9.7^{+1.2}_{-1.2}$ with $\gamma = 2.0^{+0.7}_{-0.5}$ h^{-1} Mpc, respectively. Our results are consistent with the dependence of cluster richness on the cluster correlation length.

Finally, comparing the SDSS cluster correlation function with predictions from three flat cosmological models ($\Omega_{\rm m} = 0.3$) with dark energy (quintessence), we estimate the cluster redshift-space distortion parameter $\beta \simeq \Omega_{\rm m}^{0.6}/b_0$ and the cluster bias at the present time. For the Λ cold dark matter case we find $\beta = 0.2^{+0.029}_{-0.016}$, which is in agreement with the results based on large-scale cluster motions.

Key words: galaxies: clusters: general – cosmology: theory – large-scale structure of Universe.

1 INTRODUCTION

Galaxy clusters occupy a special position in the hierarchy of cosmic structure formation, being the largest gravitationally collapsed objects in the Universe. Therefore they appear to be ideal tools for testing theories of structure formation as well as studying large-scale structure. The traditional indicator of clustering, the cluster two-point correlation function, is a fundamental statistical test for the study of the cluster distribution and is relatively straightforward to measure from observational data.

Indeed, many authors have shown, based on optical and X-ray data, that the large-scale clustering pattern of galaxy clusters is well described by a power law, $\xi(r) = (r_0/r)^\gamma$, with $\gamma = 1.6$–2. The correlation length r_0 lies in the interval $r_0 = 13$–$25\ h^{-1}$ Mpc, depending on the cluster richness as well as the analysed sample (cf. Bahcall & Soneira 1983; Klypin & Kopylov 1983; Lahav et al. 1989; Bahcall & West 1992; Peacock & West 1992; Dalton et al. 1994; Nichol, Briel & Henry 1994; Croft et al. 1997; Abadi, Lambas & Muriel 1998; Borgani, Plionis & Kolokotronis 1999; Collins et al. 2000; Moscardini, Matarrese & Mo 2001; Tago et al. 2002; Gonzalez, Zaritsky & Wechsler 2002). However, a serious issue here is how the galaxy clusters trace the underlying mass distribution. The cluster distribution traces scales that have not yet undergone the non-linear phase of gravitationally clustering, thus simplifying their connection to the initial conditions of cosmic structure formation. Galaxy clusters are strongly biased with respect to the matter distribution (e.g. Peacock & Dodds 1994 and references therein).

In this paper we utilize the recently completed Sloan Digital Sky Survey (SDSS) Cut and Enhance (CE) cluster catalogue (Goto et al. 2002) in order (i) to study the two-point correlation function in redshift space, and (ii) to calculate the relative cluster bias at the present time, comparing the observational results with those derived from three flat cosmological models with dark energy (quintessence). The structure of the paper is as follows. The observed data set and its measured correlation function are presented in Section 2. In Section 3 we give a brief account of the method used to estimate the predicted correlation function in different cold dark matter (CDM) spatially flat cosmologies. The linear growth rate of clustering in quintessence cosmological models can be found in Section 4, while in Section 5 we fit the SDSS cluster clustering to different cosmological and biasing models. Finally, we draw our conclusions in Section 6.

2 ESTIMATION OF THE SDSS CLUSTER CORRELATION FUNCTION

2.1 Cluster catalogue

In this work we use the recent SDSS CE cluster catalogue (Goto et al. 2002), which contains 2770 and 1868 galaxy clusters in the North ($145.^\circ1 < \alpha < 236.^\circ0, -1.^\circ25 < \delta < 1.^\circ25$) and South ($350.^\circ5 < \alpha < 56.^\circ61, -1.^\circ25 < \delta < 1.^\circ25$) slices respectively,

★E-mail: svasil@astro.noa.gr

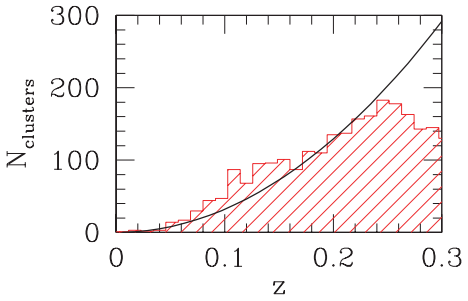

Figure 1. The estimated (histogram) and the expected (line) numbers of SDSS clusters as a function of redshift.

covering an area of ∼400 deg^2 in the sky. Redshifts are converted to proper distances using a spatially flat cosmology with $H_0 = 100\,h$ km s^{-1} Mpc^{-1} and $\Omega_m = 0.3$. The cluster redshifts are estimated using colour information by identifying the bin in $g - r$ that has the largest number of galaxies around the colour prediction of elliptical galaxies (Fukugita, Shimasaku & Ichikawa 1995) at different redshifts (which define the different $g - r$ bins). Because the true and estimated redshifts are better correlated for $z < 0.3$ (Goto et al. 2002), we will limit our analysis within this redshift range, corresponding to a limiting distance of $r_{max} \leqslant 836\,h^{-1}$ Mpc.

In Fig. 1, we present the estimated (histogram) and the expected (solid line) number of SDSS clusters as a function of redshift for a volume-limited sample. It is evident that the number of SDSS clusters appears to follow the equal-volume $\propto r^3$ law out to $z \sim 0.23$, a fact corroborated also by the standard Kolmogorov–Smirnov (KS) test which gives a probability of consistency between model and observations (up to $z \leqslant 0.23$) of $\mathcal{P}_{KS} \simeq 0.43$. Therefore this SDSS cluster sample is the only sample to date that is volume-limited to such a large distance and can thus play an important role in large-scale structure studies.

We apply the cluster correlation function analysis using clusters of two richness classes: (i) $N_{gal} \geqslant 30$ members (roughly corresponding to Abell $R \geqslant 0$; hereafter the S_1 sample) and (ii) $N_{gal} \geqslant 20$ members (roughly corresponding to Automated Plate Measuring (APM) clusters; hereafter the S_2 sample). These two subsamples contains 200 and 524 entries with corresponding mean densities of $n_{S_1}(\leqslant z_{max}) \simeq 8.42(\pm 0.06) \times 10^{-6}\,h^3$ Mpc^{-3} and $n_{S_2}(\leqslant z_{max}) \simeq 2.20(\pm 0.10) \times 10^{-5} h^3$ Mpc^{-3}, giving rise to intercluster separations of the order of $d_{S_1} \sim 49.15 \pm 2.56\,h^{-1}$ Mpc and $d_{S_2} \sim 35.66 \pm 2.18\,h^{-1}$ Mpc, respectively.

2.2 SDSS cluster correlations

We estimate the redshift-space correlation function using the estimator described by Hamilton (1993):

$$\xi_{S_j}(r) = 4\frac{N_{DD}\langle N_{RR}\rangle}{\langle N_{DR}\rangle^2} - 1, \qquad (1)$$

where $j = 1, 2$ and N_{DD} is the number of cluster pairs in the interval $[r - \Delta r, r + \Delta r]$; $\langle N_{RR}\rangle$ and $\langle N_{DR}\rangle$ are the average, over 10 000 random simulations with the same properties as the real data (boundaries and redshift selection function), numbers of cluster–random and random–random pairs, respectively. The random catalogues are constructed by randomly reshuffling the angular coordinates of the clusters (within the limits of the catalogue), while keeping the same redshifts and thus exactly the same redshift selection function as the real data.

Note that, in order to take into account the possible systematic effects (e.g. fraction of high-z clusters missed by the finding algorithm due to the SDSS magnitude limit) in the different cluster subsamples, we generate random catalogues, utilizing the individual distance distribution of each subsample and not the overall SDSS cluster selection function. We compute the errors on $\xi_{S_j}(r)$ from 100 bootstrap resamplings of the data (Mo, Jing & Börner 1992).

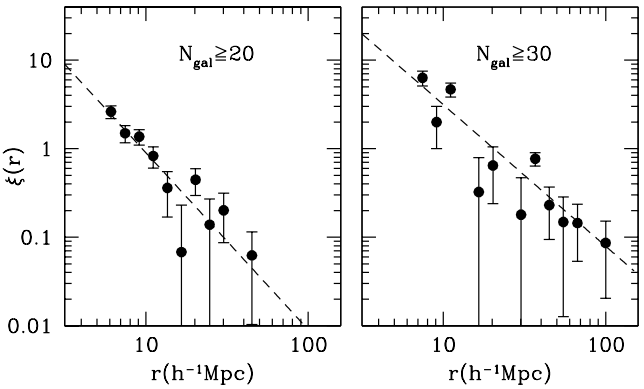

Figure 2. The spatial two-point correlation function (filled circles) in redshift space for the S_1 (Abell $R = 0$ richness, right-hand panel) and S_2 (APM richness, left-hand panel) samples. The error bars are estimated using the bootstrap procedure. The dashed lines represent the best-fitting power law $\xi_{S_j}(r) = (r_0/r)^\gamma$ (see parameters in Table 1).

We apply the correlation analysis to the S_1 and S_2 subsamples evaluating $\xi_{S_j}(r)$ in logarithmic intervals. In Fig. 2, we present the estimated two-point redshift correlation function (filled circles), divided according to richness class; strong clustering is evident. The dashed lines correspond to the best-fitting power-law model $\xi_{S_j}(r) = (r_0/r)^\gamma$, which is determined by the standard χ^2 minimization procedure in which each correlation point is weighted by the reciprocal of its error. The fit has been performed taking into account bins with $r \geqslant 5\ h^{-1}$ Mpc in order to avoid the signal from small, non-linear scales, while we have used no upper r cut-off (because of our σ^{-1} weighting scheme, our results remain robust by varying the upper r limit within the 25–100 h^{-1} Mpc range).

In Fig. 3 we present the iso-$\Delta\chi^2$ contours (where $\Delta\chi^2 = \chi^2 - \chi^2_{min}$) in the r_0–γ plane. χ^2_{min} is the absolute minimum value of

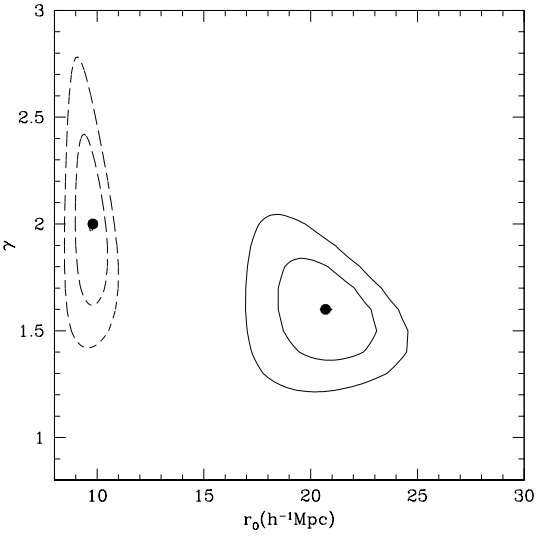

Figure 3. Iso-$\Delta\chi^2$ contours in the r_0–γ parameter space for the S_1 (continuous line) and S_2 (dashed line) samples.

Table 1. Results of the correlation function analysis for clusters of the two richness classes (S_1 and S_2 samples). Errors of the fitted parameters represent 2σ uncertainties. Finally, r_0 has units of h^{-1} Mpc.

Sample	No. of clusters	r_0	γ	$r_0(\gamma = 1.8)$
S_1	200	$20.7^{+4.0}_{-3.8}$	$\gamma = 1.6^{+0.4}_{-0.4}$	$r_0 = 19.8^{+2.9}_{-3.2}$
S_2	524	$9.7^{+1.2}_{-1.2}$	$\gamma = 2.0^{+0.7}_{-0.5}$	$r_0 = 9.8^{+1.2}_{-1.3}$

χ^2. The contours correspond to 1σ ($\Delta\chi^2 = 2.30$) and 2σ ($\Delta\chi^2 = 6.17$) uncertainties. In Table 1 we list all the relevant information. For the S_1 cluster subsample (Abell $R \geqslant 0$ richness) the best-fitting clustering parameters are $r_0 = 20.7^{+4.0}_{-3.8}\ h^{-1}$ Mpc and $\gamma = 1.6^{+0.4}_{-0.4}$ which are in very good agreement with the values $r_0 = 20.6 \pm 1.5.\ h^{-1}$ Mpc and 1.5 ± 0.2 derived by Peacock & West (1992).[1] The results for the S_2 subsample (APM richness), $r_0 = 9.7^{+1.2}_{-1.2}\ h^{-1}$ Mpc and $\gamma = 2.0^{+0.7}_{-0.5}$, can be compared with those obtained by Dalton et al. (1994) and Bahcall & West (1992), and recently by Plionis & Basilakos (2002), based on the APM cluster catalogue. They found a somewhat greater correlation length, $r_0 \simeq 12$–$13\ h^{-1}$ Mpc. We can further estimate an upper limit of the correlation length using the relation between r_0 and the mean cluster separation of Bahcall & Burgett (1986), as modified by Bahcall & West (1992): $r_{0,S_2} \simeq 0.4 d_{S_2} \simeq 14.2\, h^{-1}$ Mpc (see also Dalton et al. 1994; Croft et al. 1997).

In order to compare directly the correlation lengths of the two subsamples, we fix the correlation function slope to its nominal value of $\gamma = 1.8$ and we find $r_0 = 19.8^{+2.9}_{-3.2}$ and $9.8^{+1.2}_{-1.3}\ h^{-1}$ Mpc respectively (see the last column of Table 1). It is clear that the correlation length increases with cluster richness, as expected from the well-known richness dependence of the correlation strength.

Finally, we have investigated the isotropy of the clustering signal for both subsamples, by examining the radial and tangential components of the SDSS correlation function $\xi(\sigma, \pi)$, with π the line-of-sight separation and σ the perpendicular component of the cluster separation r (cf. Efstathiou et al. 1992). We have used bins of 20 h^{-1} Mpc width and in Fig. 4 we present $\xi(\sigma, \pi)$ for both subsamples. It is evident that the $\xi(\sigma, \pi)$ contours are elongated along the line-of-sight direction, π, up to $\sim 40\ h^{-1}$ Mpc. However, we suspect that this is not an indication of systematic effects related to line-of-sight projections, but rather due to the extremely small width of the survey area (2°.4 in the declination direction which corresponds to $\sim 25\ h^{-1}$ Mpc at a redshift of ~ 0.25), a fact that gives predominance to superclusters elongated along the line of sight with respect to those in the perpendicular direction [see Jing, Plionis & Valdarnini (1992) for the effects of superclusters elongated along the line of sight]. Below we investigate our suspicion using the *Hubble* volume ΛCDM simulation (cf. Frenk et al. 2000).

2.3 Testing the robustness of the SDSS cluster correlations

In order to test whether it is possible to recover the true underlying cluster correlations from a survey with the geometrical characteristics, selection function and richness of the SDSS, we have used the ΛCDM *Hubble* volume cluster catalogues (Colberg et al. 2000).

[1] The robustness of our results to the fitting procedure has been tested using different bins (spanning from 10 to 20) and we find very similar clustering results.

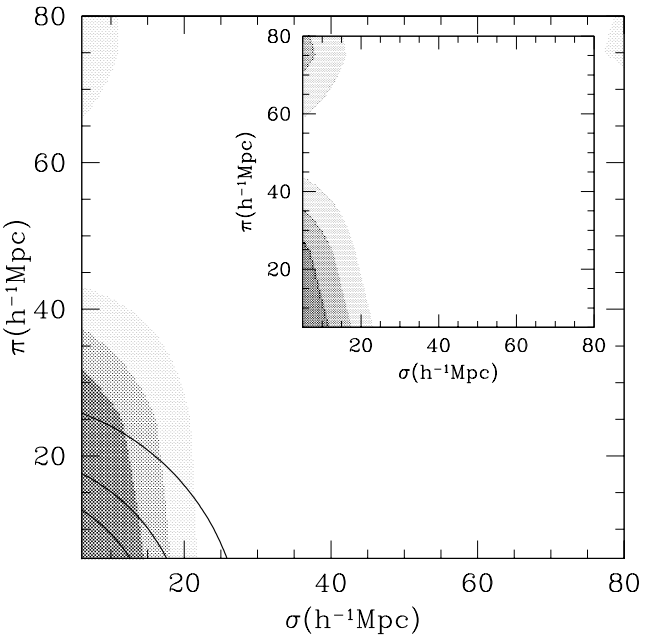

Figure 4. The radial and tangential anisotropy of the two-point correlation function of the S_1 SDSS cluster subsample (in the insert we show the results of the S_2 subsample). The transitions between different shadings correspond to fixed values of $\xi(\sigma, \pi) = 1, 0.75, 0.5$. The lines corresponds to the expected contours, using $\xi(\sigma, \pi) = [r_0/(\sigma^2 + \pi^2)]^\gamma$.

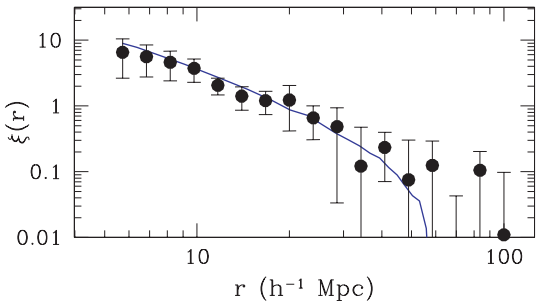

Figure 5. Comparison of the underlying ΛCDM S_1-like cluster correlation function (continuous line) with the mean of six SDSS mock samples.

As an example, we present in Fig. 5 the underlying S_1-like cluster correlation function, estimated from the whole volume (continuous line) and the mean of six mock S_1 SDSS cluster samples (which contain around 200 clusters each). The mean clustering length of the SDSS mock samples is $r_0 \simeq 18.5\ h^{-1}$ Mpc while that of the underlying cluster population is $r_0 \simeq 19.2\ h^{-1}$ Mpc. It is evident that the SDSS survey is adequate to recover the underlying clustering signal, albeit with a scatter of $\sigma(\xi)/\xi \simeq 0.3$ at separations, for example, of $r \simeq 15\ h^{-1}$ Mpc.

Furthermore, we address the issue of the observed anisotropies along the line of sight (see Fig. 4) by investigating whether mock observers show similar S_1-like clustering elongations along either their π- or σ-directions. We quantify this anisotropy by the ratio, $\mathcal{R}$, of the $\xi(\sigma, \pi)$ in the bins $(\pi, \sigma) = (0$–$20, 20$–$40)\ h^{-1}$ Mpc (hereafter $\xi_{1,2}$) and $(\pi, \sigma) = (20$–$40, 0$–$20)\ h^{-1}$ Mpc (hereafter $\xi_{2,1}$).

We have selected 114 independent mock SDSS surveys (by spanning the z coordinate axis of the simulation) and we have found that in the majority of the cases (~60 per cent) the value of $\mathcal{R}$ is

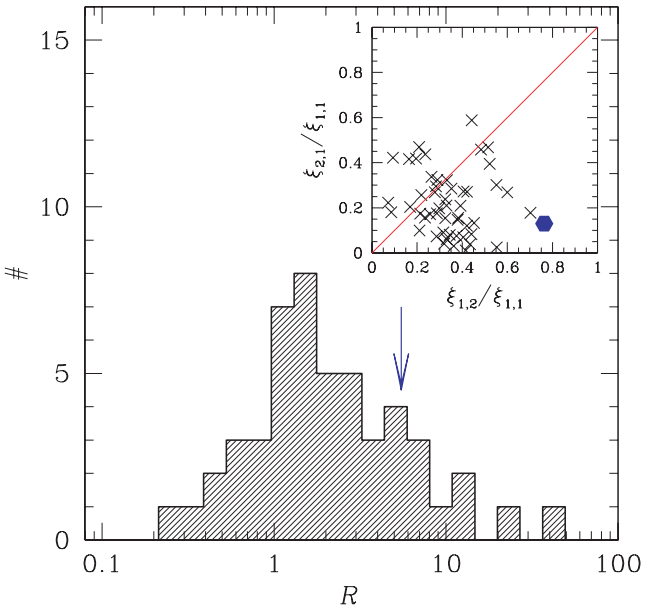

Figure 6. $\mathcal{R} = \xi_{1,2}/\xi_{2,1}$ for 50 mock S_1-like SDSS surveys for which $\xi_{1,2}$ or $\xi_{2,1}$ is larger than 0.4. Note that $\mathcal{R} > 1$ values indicate anisotropies along the π-direction, while the arrow shows the observed SDSS $\mathcal{R}$ value. The insert shows the amplitude of the anisotropies, with respect to the central value ($\xi_{1,1}$). Note that the continuous line divides anisotropies along the π-direction (right of the line) and anisotropies along the σ-direction (left of the line).

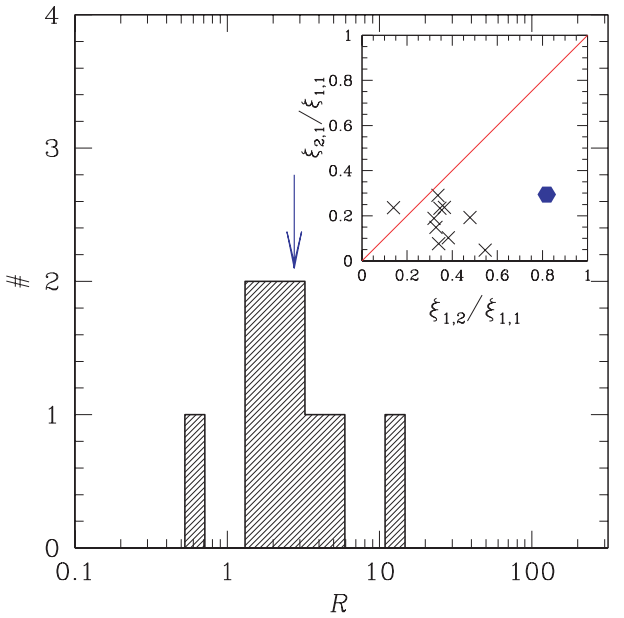

Figure 7. As in Fig. 6 but for the S_2 sample.

larger than unity, indicating a predominance of anisotropies along the π-direction, while in only ∼40 per cent of the cases is it less than 1, indicating anisotropies along the σ-direction.

We then investigated the amplitude of these S_1 clustering anisotropies by deriving the distribution of the $\mathcal{R}$ values for those observers that see relatively high correlation values: $\xi_{1,2} > 0.4$ and $\xi_{2,1} > 0.4$ (Fig. 6). In total we find 50 such observers out of which 37 (74 per cent) show elongation along their line of sight. Therefore it is evident, also because of the tail towards large $\mathcal{R}$ values, that there are systematic anisotropies along the line of sight, which of course could be only due to the geometric characteristics of the mock cluster distribution. Furthermore, in the insert of Fig. 6 we plot a scatter diagram between the normalized [by the value of $\xi(\sigma, \pi)$ at the first bin (i.e. $0 < \sigma, \pi < 20\,h^{-1}$ Mpc)] values of $\xi_{1,2}$ and $\xi_{2,1}$. It is apparent that the observed SDSS value (filled point) is roughly consistent with the simulation-derived values, although it appears to be an extremum. This indicates that the major part of the observed anisotropy is indeed due to the geometrical characteristics of the survey, as we have anticipated in the previous subsection; however, we cannot exclude the possibility that some small contribution from intrinsic systematic effects, like projection effects (cf. Sutherland 1988), could be present.

A similar analysis of the S_2 richness cluster correlations has shown that the percentage of mock observers having significant clustering anisotropies along the π-direction is significantly higher than those seeing anisotropies along the σ-direction (9 out of 10); however the amplitude of these anisotropies appears to be lower than in the observed case. In Fig. 7 we show the corresponding $\mathcal{R}$ distribution and the scatter plot, in which it is evident that the amplitude of the true SDSS clustering anisotropy in the π-direction is somewhat larger than what was expected from the survey geometrical characteristics.

Therefore we conclude that in the case of the S_1 cluster correlations there is no significant evidence for contamination by projection effects, while in the case of the S_2 correlations we do have such indications. However, in order to perform an a posteriori correction of $\xi(r)$ (cf. Efstathiou et al. 1992) for projection effects it would be necessary first to disentangle the effects of the survey geometry, a task which at the present time is beyond the scope of this work. Therefore we caution the reader that all results based on the S_2 cluster sample could be affected by the above-mentioned systematic effect.

3 MODEL CLUSTER CORRELATIONS

It is well known (cf. Kaiser 1984; Benson et al. 2000) that, assuming linear biasing, the mass tracer and dark matter correlations, at some redshift z, are related by

$$\xi_{\rm model}(r, z) = \xi_{\rm DM}(r, z) b^2(z), \tag{2}$$

where $b(z)$ is the bias redshift evolution function. In the present work we have used the so-called test particle bias model described by Nusser & Davis (1994), Fry (1996) and Tegmark & Peebles (1998). In this case the evolution of the correlation bias is developed assuming that only the test particle fluctuation field is related proportionally to that of the underlying mass. Therefore the bias factor as a function of redshift is

$$b(z) = 1 + \frac{(b_0 - 1)}{D(z)}, \tag{3}$$

with b_0 being the bias at the present time and $D(z)$ the linear growth rate of clustering (described in Section 4). It has been found (Bagla 1998) that, in the interval $0 \leqslant z \leqslant 1$, the above formula represents the evolution of bias well. Furthermore, the more accurate linear bias evolution model given by Basilakos & Plionis (2001, 2003) is also very similar to the model of equation (3) within $z \leqslant 1$.

We quantify the evolution of clustering with epoch, presenting the spatial correlation function of the mass $\xi_{\rm DM}(r, z)$ as the Fourier

transform of the spatial power spectrum $P(k)$:

$$\xi_{\rm DM}(r,z) = D^2(z)\frac{1}{2\pi^2}\int_0^\infty k^2 P(k)\frac{\sin(kr)}{kr}{\rm d}k, \quad (4)$$

where k is the comoving wavenumber.

As for the power spectrum, we consider that of CDM models, where $P(k) \approx k^n T^2(k)$ with scale-invariant ($n = 1$) primeval inflationary fluctuations. We utilize the transfer function parametrization as in Bardeen et al. (1986), with the approximate corrections given by Sugiyama's (1995) formula:

$$T(k) = \frac{\ln(1+2.34q)}{2.34q}[1+3.89q+(16.1q)^2 + (5.46q)^3+(6.71q)^4]^{-1/4}$$

with

$$q = \frac{k}{\Omega_0 h^2 \exp[-\Omega_{\rm b} - (2h)^{1/2}\Omega_{\rm b}/\Omega_0]}, \quad (5)$$

where $k = 2\pi/\lambda$ is the wavenumber in units of h Mpc^{-1} and $\Omega_{\rm b}$ is the baryon density.

In the present analysis we consider flat models with cosmological parameters that fit the majority of observations, i.e. $\Omega_{\rm m} + \Omega_{\rm Q} = 1$, $H_0 = 100\ h$ km s^{-1} Mpc^{-1} with $h \simeq 0.7$ (cf. Freedman et al. 2001; Plionis 2002; Peebles & Ratra 2003, and references therein), baryonic density parameter $\Omega_{\rm b}h^2 \simeq 0.02$ (e.g. Olive, Steigman & Walker 2000; Kirkman et al. 2003) and a CDM shape parameter $\Gamma = 0.17$. In particular, we investigate three spatially flat low-$\Omega_{\rm m} = 0.3$ cosmological models with negative pressure and values of $w = -1$ (ΛCDM), $w = -2/3$ (QCDM1) and $w = -1/3$ (QCDM2). Note that all the cosmological models are normalized to have a fluctuation amplitude, in a sphere of 8 h^{-1} Mpc radius, of $\sigma_8 = 0.50\ (\pm 0.1)$ $\Omega_{\rm m}^{-\gamma}$ (Wang & Steinhardt 1998) with $\gamma = 0.21 - 0.22w + 0.33\Omega_{\rm m}$.

4 THE LINEAR GROWTH RATE OF CLUSTERING

For homogeneous and isotropic flat cosmologies, driven by non-relativistic matter and an exotic fluid (quintessence models) with equation of state $p_{\rm Q} = w\rho_{\rm Q}$ and $-1 \leqslant w < 0$, the Friedmann field equations can be written as

$$H^2 = \left(\frac{\dot\alpha}{\alpha}\right)^2 = \frac{8\pi G}{3}(\rho_{\rm m} + \rho_{\rm Q}) \quad (6)$$

and

$$\frac{\ddot\alpha}{\alpha} = -4\pi G\left[\left(w+\frac{1}{3}\right)\rho_{\rm Q} + \frac{1}{3}\rho_{\rm m}\right], \quad (7)$$

where $\alpha(t)$ is the scale factor, $\rho_{\rm m} \propto \alpha(t)^{-3}$ is the matter density and $\rho_{\rm Q} \propto \alpha(t)^{-3(1+w)}$ is the dark energy density.

The time evolution equation for the mass density contrast, modelled as a pressureless fluid, has a general solution of the growing mode (Peebles 1993):

$$\ddot D + 2H(t)\dot D = 4\pi G\rho_{\rm m} D, \quad (8)$$

where dots denote derivatives with respect to time. From the equations describing the Friedmann model, it follows that $\dot H + H^2 = -4\pi G[(w+1/3)\rho_{\rm Q} + (1/3)\rho_{\rm m}]$. Differentiating this relation and using $\dot\rho_{\rm m} = -3H\rho_{\rm m}$, $\dot\rho_{\rm Q} = -3(1+w)H\rho_{\rm Q}$, we obtain

$$\ddot H + 2H\dot H = 4\pi G(1+w)\left(w+\frac{1}{3}\right)\rho_{\rm Q}H + 4\pi G\rho_{\rm m}H. \quad (9)$$

Therefore it turns out that if $w = -1$ (ΛCDM) or $w = -1/3$ (QCDM2) then $H(t)$ is a decaying mode of equation (8). In that case, the growing solution (Peebles 1993) as a function of redshift is

$$D(z) = \frac{5\Omega_{\rm m}E(z)}{2}\int_z^\infty \frac{(1+x)}{E^3(x)}{\rm d}x, \quad (10)$$

where we have used the following expressions:

$$E(z) = \left[\Omega_{\rm m}(1+z)^3 + \Omega_{\rm Q}(1+z)^{3(1+w)}\right]^{1/2}, \quad (11)$$

$$\frac{{\rm d}t}{{\rm d}z} = -\frac{1}{H_0 E(z)(1+z)}. \quad (12)$$

The Hubble parameter is given by $H(z) = H_0E(z)$, while $\Omega_{\rm m} = 8\pi\ G\ \rho_0/3H_0^2$ (density parameter) and $\Omega_{\rm Q} = 8\pi\ G\ \rho_{\rm Q}/3H_0^2$ (dark energy parameter) at the present time, which satisfy $\Omega_{\rm m} + \Omega_{\rm Q} = 1$, and finally H_0 is the Hubble constant. In addition to $\Omega_{\rm m}(z)$, also $\Omega_{\rm Q}(z)$ could evolve with redshift as

$$\Omega_{\rm m}(z) = \frac{\Omega_{\rm m}(1+z)^3}{E^2(z)} \quad (13)$$

and

$$\Omega_{\rm Q}(z) = \frac{\Omega_{\rm Q}(1+z)^{3(1+w)}}{E^2(z)}. \quad (14)$$

It is of interest to mention that in a flat low-$\Omega_{\rm m}$ model with $w = -1/3$, the equation of state $p_{\rm Q} = -(1/3)\rho_{\rm Q}$ leads to the same growing mode as in an open universe, despite the fact that this quintessence model has a spatially flat geometry! Therefore, as time evolves with redshift, utilizing equations (12) and (11) and the relation

$$4\pi G\rho_{\rm m} = \frac{3H_0^2}{2}\Omega_{\rm m}(1+z)^3, \quad (15)$$

then the basic differential equation for the evolution of the linear growing mode takes the following form:

$$\frac{{\rm d}^2D}{{\rm d}z^2} + P(z)\frac{{\rm d}D}{{\rm d}z} + Q(z)D = 0, \quad (16)$$

with basic factors

$$P(z) = -\frac{1}{1+z} + \frac{1}{E(z)}\frac{{\rm d}E(z)}{{\rm d}z} \quad (17)$$

and

$$Q(z) = \frac{3\Omega_{\rm m}(1+z)}{2E^2(z)}. \quad (18)$$

We find that equation (15) has a decaying solution of the form $D_1(z) = (1+z)^n$ only for $w = -2/3$, with $n = 3/2$. The second independent solution of equation (16) can be found easily from the following expression:

$$D(z) = D_1(z)\int_z^\infty \frac{{\rm d}x}{D_1^2(x)}\exp\left[-\int^x P(t){\rm d}t\right], \quad (19)$$

which finally leads to the following growing mode:

$$D(z) = (1+z)^{3/2}\int_z^\infty \frac{{\rm d}x}{(1+x)^2E(x)}. \quad (20)$$

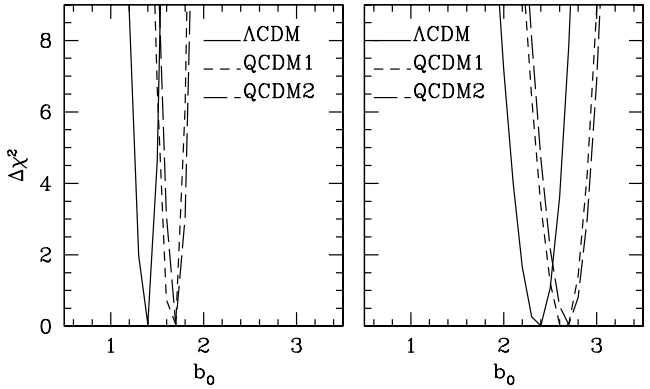

Figure 8. The variance $\Delta\chi^2$ around the best-fitting b_0 value for various cosmological models. The left- and right-hand panels correspond to the S_2 and S_1 samples, respectively.

Table 2. The theoretical clustering model fitting analysis. Note that the errors of the fitted parameters represent 2σ uncertainties.

Index	b_0	β	$K(\beta)$
ΛCDM-S_1	$2.4^{+0.2}_{-0.3}$	$0.20^{+0.029}_{-0.016}$	$1.14^{+0.02}_{-0.01}$
QCDM1-S_1	$2.6^{+0.3}_{-0.2}$	$0.19^{+0.016}_{-0.020}$	$1.13^{+0.01}_{-0.01}$
QCDM2-S_1	$2.7^{+0.2}_{-0.3}$	$0.18^{+0.023}_{-0.013}$	$1.12^{+0.02}_{-0.01}$
ΛCDM-S_2	$1.4^{+0.1}_{-0.1}$	$0.35^{+0.027}_{-0.023}$	$1.26^{+0.02}_{-0.02}$
QCDM1-S_2	$1.7^{+0.1}_{-0.1}$	$0.29^{+0.019}_{-0.019}$	$1.21^{+0.01}_{-0.01}$
QCDM2-S_2	$1.7^{+0.1}_{-0.1}$	$0.30^{+0.019}_{-0.016}$	$1.22^{+0.01}_{-0.01}$

5 THE SDSS CLUSTER BIASING

In order to quantify the cluster bias at the present time, we perform a standard χ^2 minimization procedure (described before) between the measured correlation function of the SDSS galaxy clusters and those expected in our spatially flat cosmological models:

$$\chi^2(b_0) = \sum_{i=1}^{n} \left[\frac{\xi^i_{S_j}(r) - \xi^i_{\rm model}(r, b_0)}{\sigma^i} \right]^2, \qquad (21)$$

where σ^i is the observed correlation function (bootstrap) uncertainty.

In Fig. 8 we present, for various cosmological models, the variation of $\Delta\chi^2 = \chi^2(b_0) - \chi^2_{\rm min}(b_0)$ around the best b_0 fit, for the different richness classes (left-hand panel for S_2 and right-hand panel for S_1).

To this end, owing to the fact that the observational data are analysed in redshift space, the correlations should be amplified by the factor $K(\beta) = 1 + 2\beta/3 + \beta^2/5$ (Hamilton 1992), where $\beta \simeq \Omega^{\alpha}_{\rm m}/b_0$. We utilize the generic expression for α, defined by Wang & Steinhardt (1998):

$$\alpha \simeq \frac{3}{5 - w/(1-w)} + \frac{3}{125}\frac{(1-w)(1-3w/2)}{(1-6w/5)^3}(1-\Omega_{\rm m}). \qquad (22)$$

In Table 2 we list the results of the fits for our two cluster catalogues, i.e. the cosmological models and the value of the cluster optical bias, b_0, at the present time, as well as the redshift distortion β parameter and a measure of the $K(\beta)$ correction. We find that the redshift-space distortion effect increases $\xi_{S_j}(r)$ by ~12–26 per cent.

In Fig. 9, we plot the measured $\xi_{S_j}(r)$ (filled symbols) of our two samples with the estimated two-point correlation function for

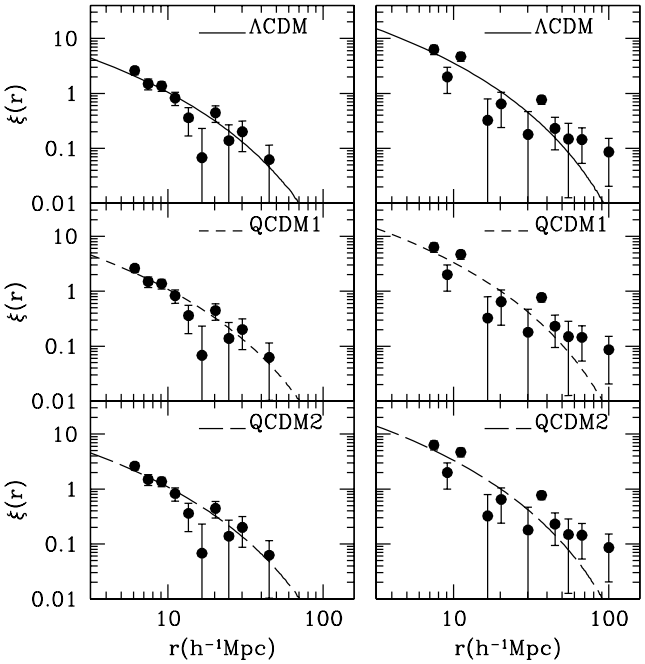

Figure 9. Comparison of the observed and model SDSS cluster correlation functions: left-hand panel, S_2 sample; right-hand panel, S_1 sample. The observational data are represented by filled symbols.

all three cosmological models. We conclude that the behaviour of the observed two-point correlation function of the galaxy clusters is sensitive to the different cosmologies with a strong dependence on the present time bias. By distinguishing between low- and high-richness regimes, we obtain results consistent with the hierarchical clustering scenario, in which the rich clusters are more biased tracers of the underlying matter distribution with respect to the low-richness clusters.

We can deduce some further cosmological constraints, by comparing our clustering results with those based on large-scale dynamics. For example, Branchini & Plionis (1996), using the cluster dipole after reconstructing the spatial distribution of Abell/ACO $R \geqslant 0$ clusters, found $\beta_{\rm Abell} = 0.21 \pm 0.03$. Also, Branchini et al. (2000), comparing the density and velocity fields of the Abell/ACO cluster distribution with the corresponding POTENT-reconstructed fields (using the MARK III galaxy velocity sample), obtained $\beta_{\rm POTENT} = 0.22 \pm 0.08$. Comparing the latter β results with our clustering predictions (Table 2), we can conclude that for the S_1 sample (Abell $R \geqslant 0$ richness) the only model that fails (although marginally) to reproduce the large-scale dynamical results is QCDM2 ($w = -1/3$).

6 CONCLUSIONS

We have studied the clustering properties of the SDSS galaxy clusters in redshift space. We have divided the total sample into two richness subsamples, roughly corresponding to Abell $R \geqslant 0$ ($N_{\rm gal} \geqslant 30$ members) and to APM ($N_{\rm gal} \geqslant 20$ members) clusters. We find that if the two-point cluster correlation function is modelled as a power law, $\xi(r) = (r_0/r)^{\gamma}$, then the best-fitting parameters are (i) $r_0 = 20.7^{+4.0}_{-3.8}\ h^{-1}$ Mpc with $\gamma = 1.6^{+0.4}_{-0.4}$, and (ii) $r_0 = 9.7^{+1.2}_{-1.2}\ h^{-1}$ Mpc with $\gamma = 2.0^{+0.7}_{-0.5}$, respectively. We have also found that the Abell-like sample is not significantly affected by projection effects, and its apparent clustering elongation along the line of sight is due

to the survey geometry. However, the APM-like sample appears to be somewhat affected by projection effects, showing a clustering elongation along the line of sight larger than what is expected from the survey geometry.

Comparing the cluster correlation function with the predictions of three spatially flat quintessence models (having $\Omega_{\rm m} = 0.3$), we estimate the cluster redshift-space distortion parameter $K(\beta)$ and we conclude that the amplitude of the cluster redshift correlation function increases by $\sim$12–26 per cent (depending on the richness class). Finally, comparing our clustering results with those of dynamical analysis, based on the large-scale motions, we find that the flat cosmological models with $w \leqslant -0.6$ are consistent with the observational results.

ACKNOWLEDGMENTS

The ΛCDM simulation used in this paper was carried out by the Virgo Supercomputing Consortium using computers based at the Computing Centre of the Max Planck Society in Garching and at the Edinburgh Parallel Computing Centre. The data are publicly available at http://www.mpa-garching.mpg.de/NumCos. This work is jointly funded by the European Union and the Greek Government in the framework of the programme 'Promotion of Excellence in Technological Development and Research', project 'X-ray Astrophysics with ESA's mission XMM'. Furthermore, MP acknowledges support by the Mexican Government grant No CONACyT-2002-C01-39679. Finally, we thank the referee, Chris Collins, for useful suggestions.

REFERENCES

Abadi M. G., Lambas D. G., Muriel H., 1998, ApJ, 507, 526
Bagla J. S., 1998, MNRAS, 417, 424
Bahcall N., Burgett W. S., 1986, ApJ, 300, L35
Bahcall N., Soneira R. M., 1983, ApJ, 270, 20
Bahcall N., West M. J., 1992, ApJ, 392, 419
Bardeen J. M., Bond J. R., Kaiser N., Szalay A. S., 1986, ApJ, 304, 15
Basilakos S., Plionis M., 2001, ApJ, 550, 522
Basilakos S., Plionis M., 2003, ApJ, 593, L61
Benson A. J., Cole S., Frenk S. C., Baugh M. C., Lacey G. C., 2000, MNRAS, 311, 793
Borgani S., Plionis M., Kolokotronis V., 1999, MNRAS, 305, 866
Branchini E., Plionis M., 1996, ApJ, 460, 569
Branchini E., Zehavi I., Plionis M., Dekel A., 2000, MNRAS, 313, 491
Colberg J. M. et al., 2000, MNRAS, 319, 209
Collins C. A. et al., 2000, MNRAS, 319, 939
Croft R. A. C., Dalton B., Efstathiou G., Sutherland W. J., Maddox S. J., 1997, MNRAS, 291, 305
Dalton B. G., Croft R. A. C., Efstathiou G., Sutherland W. J., Maddox S. J., Davis M., 1994, MNRAS, 271, L47
Efstathiou G., Dalton B. G., Sutherland W. J., Maddox S. J., 1992, MNRAS, 257, 125
Freedman W. L. et al., 2001, ApJ, 553, 47
Frenk C. S. et al., 2000, preprint (astro-ph/0007362)
Fry J. N., 1996, ApJ, 461, 65
Fukugita M., Shimasaku K., Ichikawa T., 1995, PASP, 107, 945
Gonzalez A. H., Zaritsky D., Wechsler R. H., 2002, ApJ, 571, 129
Goto T. et al., 2002, AJ, 123, 1825
Hamilton A. J. S., 1992, ApJ, 385, L5
Hamilton A. J. S., 1993, ApJ, 417, 19
Jing Y. P., Plionis M., Valdarnini R., 1992, ApJ, 389, 499
Kaiser N., 1984, ApJ, 284, L9
Kirkman D., Tytler D., Suzuki N., O'Meara J. M., Lubin D., 2003, ApJS, 149, 1
Klypin A. A., Kopylov A. I., 1983, Sov. Astron. Lett., 9, 41
Lahav O., Edge A. C., Fabian A. C., Putney A., 1989, MNRAS, 238, 881
Mo H. J., Jing Y. P., Börner G., 1992, ApJ, 392, 452
Moscardini L., Matarrese S., Mo H. J., 2001, MNRAS, 327, 422
Nichol R. C., Briel O. G., Henry P. J., 1994, ApJ, 267, 771
Nusser A., Davis M., 1994, ApJ, 421, L1
Olive K. A., Steigman G., Walker T. P., 2000, Phys. Rep., 333, 389
Peacock A. J., Dodds S. J., 1994, MNRAS, 267, 1020
Peacock A. J., West M., 1992, MNRAS, 259, 494
Peebles P. J. E., 1993, Principles of Physical Cosmology. Princeton Univ. Press, Princeton, NJ
Peebles P. J. E., Ratra B., 2003, Rev. Mod. Phys., 75, 559
Plionis M., 2002, in Cotsakis S., Papandonopoulos E., eds, Lecture Notes in Physics Vol. 592, Cosmological Crossroads. Springer, Berlin, p. 147
Plionis M., Basilakos S., 2002, MNRAS, 329, L47
Sugiyama N., 1995, ApJS, 100, 281
Sutherland W., 1988, MNRAS, 234, 159
Tago E., Saar E., Einasto J., Einasto M., Müller V., Andernach H., 2002, AJ, 123, 37
Tegmark M., Peebles P. J. E., 1998, ApJ, 500, L79
Wang L., Steinhardt P. J., 1998, ApJ, 508, 483

This paper has been typeset from a TEX/LATEX file prepared by the author.